Electronic Supplementary Information for

Facile synthesis Carbon nanofibers confined FeS_2/Fe_2O_3 heterostructures as superior anode material for sodium-ion battery

Shuaiguo Zhang [a]*, guoyou Yin [b], Haipeng Zhao [a], Jie Mi [c], Jie Sun [b], Liyun Dang [a]

[a] College of Material and Chemical Engineering, Henan University of Urban Construction, Pingdingshan 467036, PR China

[b] College of Life Science and Technology, Henan University of Urban Construction, Henan University of Urban Construction, Pingdingshan 467036, PR China

c Key Laboratory of Coal Science and Technology of Shanxi Province and Ministry of Education, Taiyuan University of Technology, Taiyuan 030024, Shanxi, China.

Corresponding author: Shuaiguo Zhang

E-mail address: zhangguoyuan.1234@163.com.

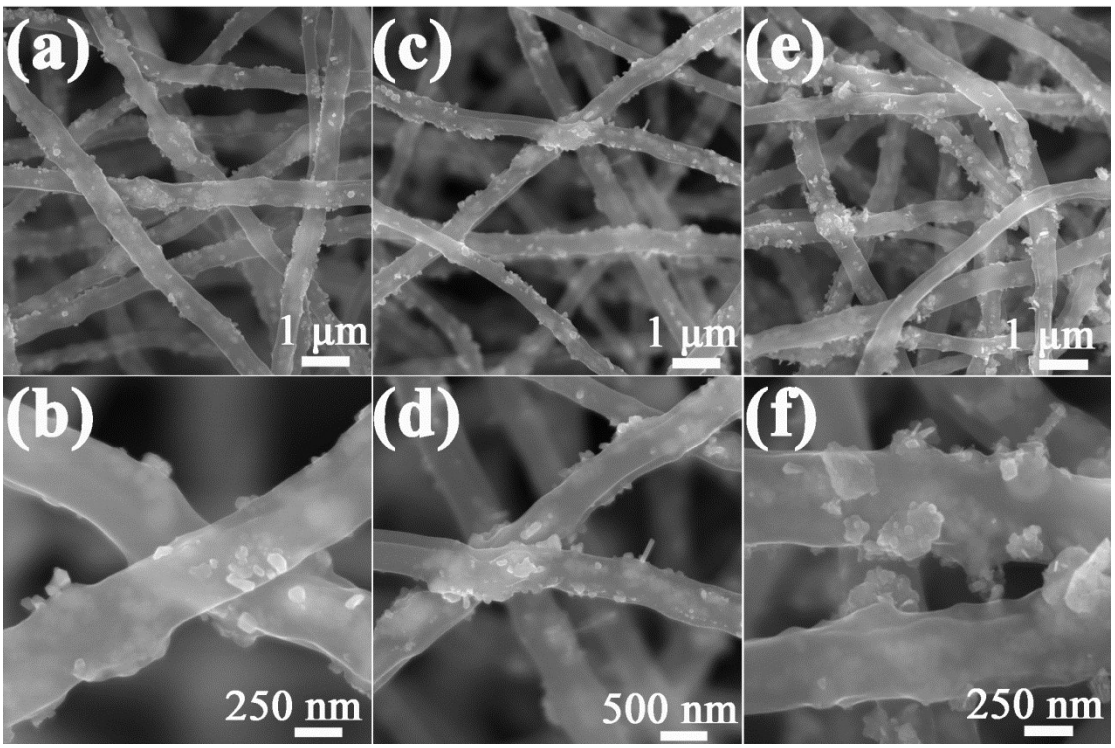

Fig. S1. SEM images of the as-obtained FeS_2/Fe_2O_3@N-CNFs with different sulfuration time (a, b) 1-Fe_2O_3@N-CNFs, (c, d) 2-FeS_2/Fe_2O_3@N-CNFs and (e, f) 3-FeS_2/Fe_2O_3@N-CNFs.

Detailed calculation process of the relative contents in 2-FeS_2/Fe_2O_3@N-CNFs composite is presented as below. The relative content of CNFs in 2-FeS_2/Fe_2O_3@N-CNFs composite is 36.9%, which can be directly estimated from the TGA curve. The relative content of FeS_2 can be obtained from the following equation:

$$2FeS_2 \rightarrow Fe_2O_3 \sim \Delta S$$
$$239.9\ \text{g/mol} \rightarrow 159.7\ \text{g/mol} \sim 80.2\ \text{g/mol}$$

$$\frac{\Delta S}{80.2\ \text{g/mol}} = \frac{x}{239.9\ \text{g/mol}}$$

Where x is weight percentage of FeS_2, 80.2 g/mol represent the stoichiometric weight loss from FeS_2 to Fe_2O_3. ΔS is weight loss from FeS_2 to Fe_2O_3 (9.3% in this work). Therefore, the calculated relative content of FeS_2 is 27.8%, and the relative content of Fe_2O_3 is 35.3%.

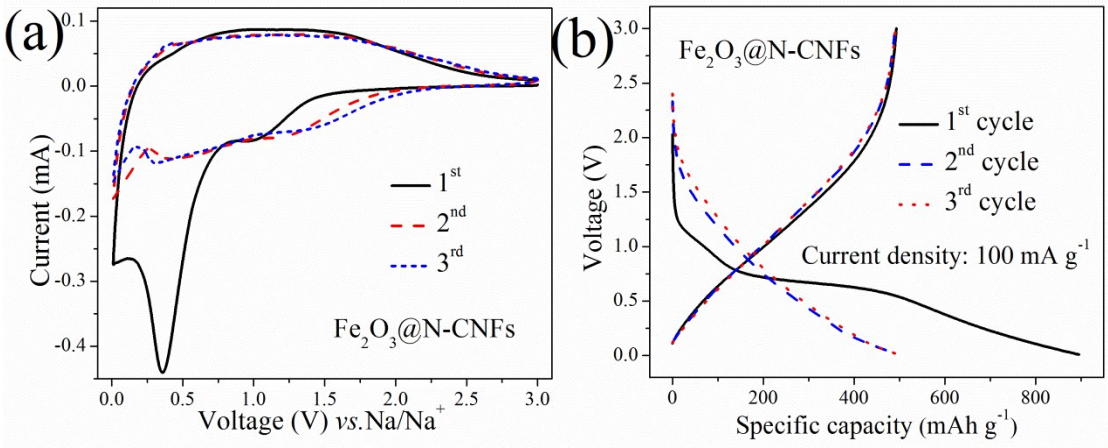

Fig. S2. (a) CV curves and (b) galvanostatic charge/discharge profiles of Fe_2O_3@N-CNFs electrode.

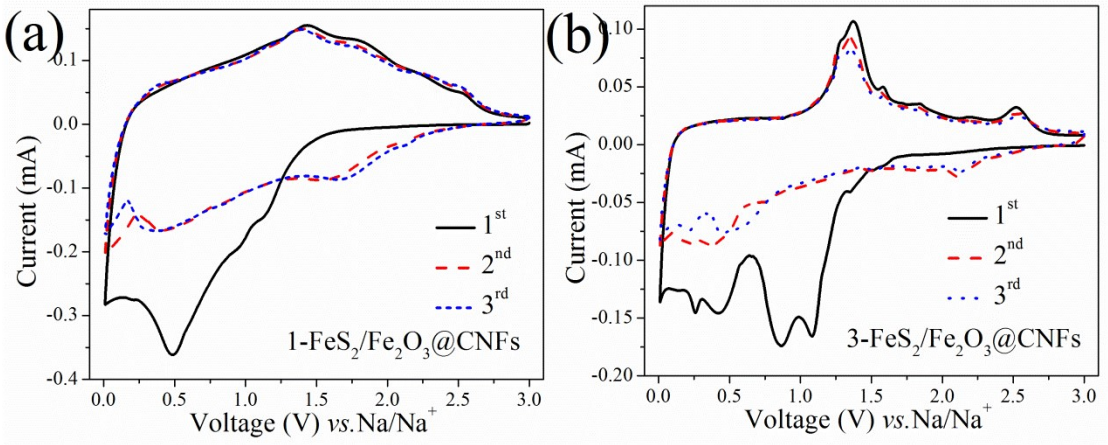

Fig. S3. (a) CV curves of 1-FeS_2/Fe_2O_3@N-CNFs and 3-FeS_2/Fe_2O_3@N-CNFs obtained at scan rate of 0.1 mV s^{-1}.

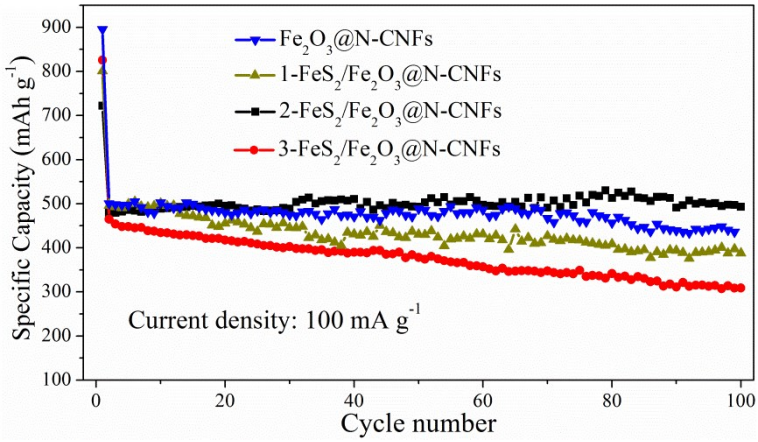

Fig. S4. Cyclic performance of the as-obtained samples in a voltage window of 0.01-3.0 V with a current density of 100 mA g^{-1}.

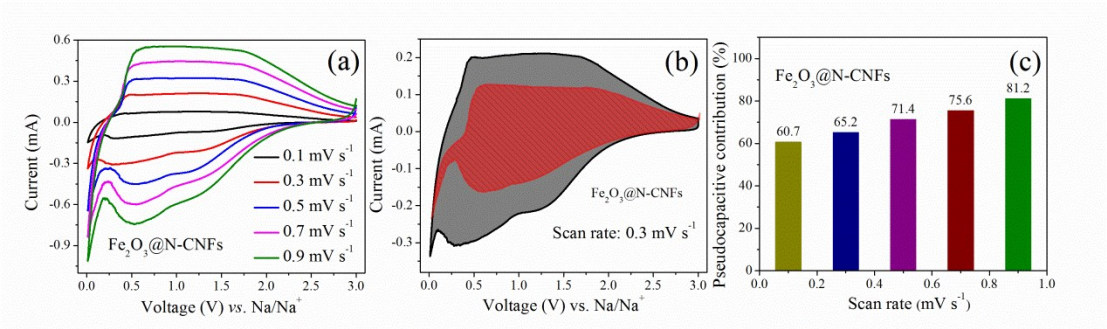

Fig. S5. (a) CV curves of Fe_2O_3@N-CNFs electrode with different scan rates; (b) the calculated capacitive current contribution from the CV curves at scan rate of 0.3 mV s^{-1}; (c) the psudocapacitive contribution proportion of Fe_2O_3@N-CNFs at different scan rates.

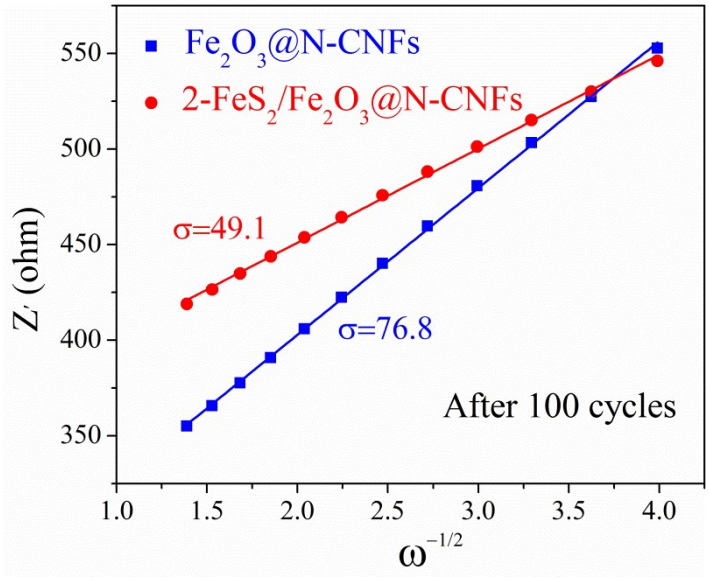

Fig. S6. Linear relationship of the real impedance against the minus square root of the frequency

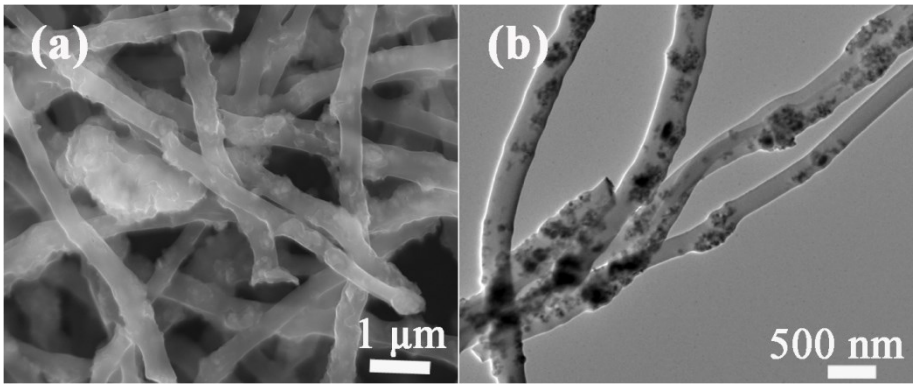

Fig. S7. SEM (a) and TEM (b) images of Fe_2O_3@N-CNFs electrode obtained after 600 cycles at current density of 1 A g^{-1}.

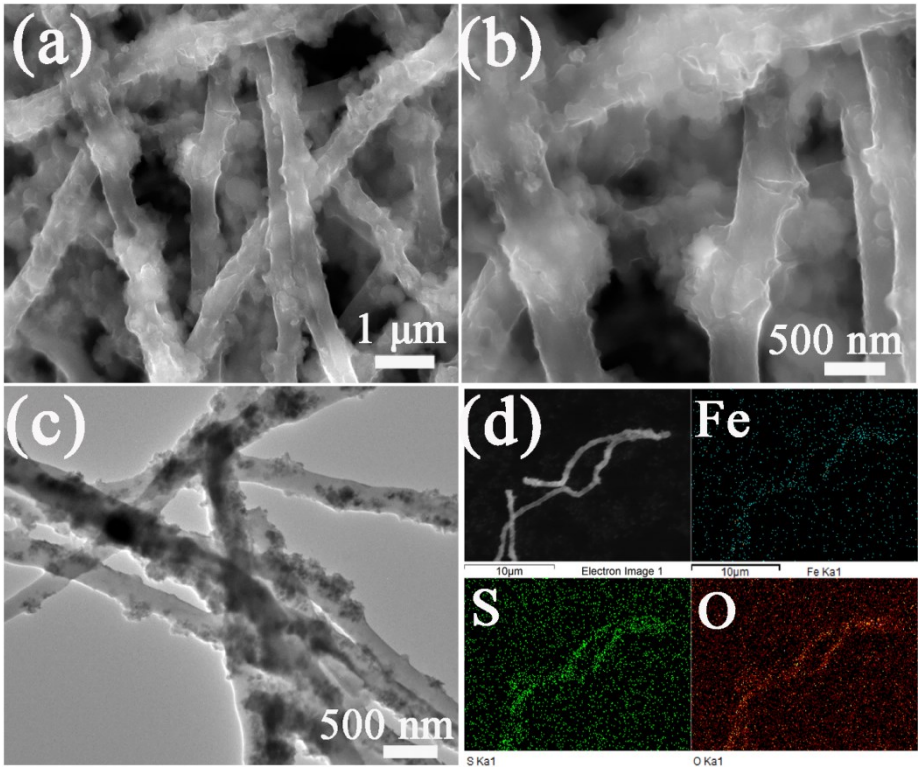

Fig. S8. Typical SEM (a, b) and TEM (c) images of 2-FeS_2/Fe_2O_3@N-CNFs electrodes after 600 cycles with different magnification; (d) SEM elemental mapping images of the cycled 2-FeS_2/Fe_2O_3@N-CNFs fibers.

Table. S1. Comparison of sodium storage performances of 2-FeS_2/Fe_2O_3@N-CNFs electrodes in this work and previously reported Fe-based anodes.

Sample	Cycling performance (mAh g^{-1})			Rate capacity (mAh g^{-1})
	1st (mAh g^{-1})	Cycle number	Capacity after cycles (mAh g^{-1})	
2-FeS_2/Fe_2O_3@N-CNFs (This work)	454.6 at 0.1 A g^{-1}	600	287.3 at 1 A g^{-1}	246.2 at 1.6 A g^{-1}
Fe_7S_8@NC[1]	468 at 0.1 A g^{-1}	50	/	403 at 2 A g^{-1}
Fe_7S_8@S/N–C[2]	/	150	274 at 1 A g^{-1}	280 at 2 A g^{-1}
Fe_7S_8/N-Gr [3]	/	500	393.1 at 0.4 A g^{-1}	543 at 10 A g^{-1}
Fe_3O_4@FeS[4]	215 at 0.05 A g^{-1}	750	169 at 0.2 A g^{-1}	151 at 2 A g^{-1}
Fe_2O_3@rGO [5]	610 at 0.05 A g^{-1}	100	~500 at 0.05 A g^{-1}	216 at 2 A g^{-1}
FeS_2@C [6]	/	400	203.5 at 10 A g^{-1}	200 at 10 A g^{-1}
$Fe_{1-x}S$@CNTs[7]	478.7 at 0.2 A g^{-1}	200	449.2 at 0.5 A g^{-1}	326.3 at 8 A g^{-1}
Fe_2O_3@N-CNFs [8]	/	350	408 at 0.1 A g^{-1}	183 at 3 A g^{-1}
Fe_2O_3/C [9]	423.8 at 0.05 A g^{-1}	300	101.9 at 2 A g^{-1}	166 at 2 A g^{-1}
FeS_2@rGO [10]	/	250	245 at 0.1875 A g^{-1}	192.9 at 0.75 A g^{-1}
Fe_7S_8/C [11]	/	100	497 at 0.1 A g^{-1}	/
FeO_x/CNFs [12]	/	500	277 at 0.5 A g^{-1}	169 at 4 A g^{-1}
FeS/g-C [13]	/	180	742.9 at 0.05 A g^{-1}	647.1 at 4 A g^{-1}
C/FeS [14]	661 at 0.2 A g^{-1}	200	265 at 1 A g^{-1}	260 at 1 A g^{-1}
FeS_2/CNT [15]	/	400	394 at 0.2 A g^{-1}	254 at 22 A g^{-1}
$Fe_{1-x}S$ [16]	617 at 0.1 A g^{-1}	200	563 at 0.1 A g^{-1}	300 at 10 A g^{-1}
FeS_2/FeS [17]	742 at 0.1 A g^{-1}	100	513 at 0.1 A g^{-1}	284 at 20 A g^{-1}
Fe_7S_8/carbon [18]	1005.3 at 0.2 A g^{-1}	200	654 at 2 A g^{-1}	335.2 at at 2 A g^{-1}

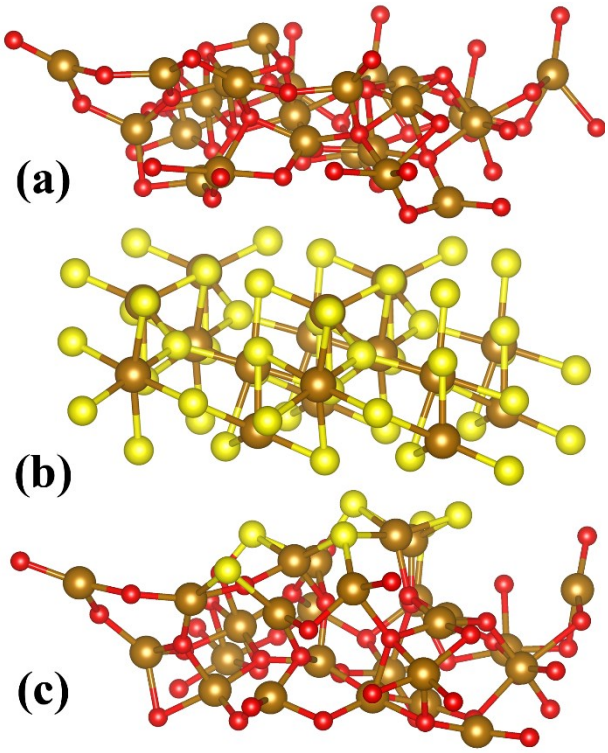

Fig. S9. Optimized geometry structures of (a) Fe_2O_3, (b) FeS_2 and (c) Fe_2O/FeS_2 heterostructure.

References:

[1] Zhou Y, Zhang M, Wang Q, et al. Pseudocapacitance boosted N-doped carbon coated Fe_7S_8 nanoaggregates as promising anode materials for lithium and sodium storage[J]. Nano Research, 2020, 13: 691-700.

[2] Li X, Liu T, Wang Y-X, et al. S/N-doped carbon nanofibers affording Fe_7S_8 particles with superior sodium storage[J]. Journal of Power Sources, 2020, 451: 227790.

[3] He Q, Rui K, Yang J, et al. Fe_7S_8 Nanoparticles Anchored on Nitrogen-Doped Graphene Nanosheets as Anode Materials for High Performance Sodium Ion Batteries[J]. ACS Applied Materials & Interfaces, 2018, 10(35): 29476-29485.

[4] Hou B, Wang Y, Guo J, et al. A Scalable Strategy To Develop Advanced Anode for Sodium-Ion Batteries: Commercial Fe_3O_4-Derived Fe_3O_4@FeS with Superior Full-Cell Performance[J]. ACS Applied Materials & Interfaces, 2018, 10(4): 3581-3589.

[5] Li T, Qin A, Yang L, et al. In Situ Grown Fe_2O_3 Single Crystallites on Reduced Graphene Oxide Nanosheets as High Performance Conversion Anode for Sodium-Ion Batteries[J]. ACS Applied Materials & Interfaces, 2017, 9(23): 19900-19907.

[6] Shao M, Cheng Y, Zhang T, et al. Designing MOFs-Derived FeS_2@Carbon Composites for High-Rate Sodium Ion Storage with Capacitive Contributions[J]. ACS Applied Materials & Interfaces, 2018, 10(39): 33097-33104.

[7] Xiao Y, Hwang J, Belharouak I, et al. Na Storage Capability Investigation of a Carbon Nanotube-Encapsulated $Fe_{1-x}S$ Composite[J]. ACS Energy Letters, 2017, 2(2): 364-372.

[8] Shi L, Li Y, Zeng F, et al. In situ growth of amorphous Fe_2O_3 on 3D interconnected nitrogen-doped carbon nanofibers as high-performance anode materials for sodium-ion batteries[J]. Chemical Engineering Journal, 2019, 356: 107-116.

[9] Li M, Ma C, Zhu Q C, et al. Well-ordered mesoporous Fe_2O_3/C composites as high performance anode materials for sodium-ion batteries[J]. Dalton Trans, 2017, 46(15): 5025-5032.

[10] Chen W, Qi S, Yu M, et al. Design of FeS_2@rGO composite with enhanced rate and cyclic performances for sodium ion batteries[J]. Electrochimica Acta, 2017, 230: 1-9.

[11] Li S, Qu B, Huang H, et al. Controlled synthesis of iron sulfide coated by carbon layer to improve lithium and sodium storage[J]. Electrochimica Acta, 2017, 247: 1080-1087.

[12] Xu Z, Yao S, Cui J, et al. Atomic scale, amorphous FeO_x/carbon nanofiber anodes for Li-ion and Na-ion batteries[J]. Energy Storage Materials, 2017, 8: 10-19.

[13] Fan H, Li H, Guo J, et al. Target construction of ultrathin graphitic carbon encapsulated FeS hierarchical microspheres featuring superior low-temperature lithium/sodium storage properties[J]. Journal of Materials Chemistry A, 2018, 6(17): 7997-8005.

[14] Cao Z, Song H, Cao B, et al. Sheet-on-sheet chrysanthemum-like C/FeS microspheres synthesized by one-step solvothermal method for high-performance sodium-ion batteries[J]. Journal of Power Sources, 2017, 364: 208-214.

[15] Chen Y, Hu X, Evanko B, et al. High-rate FeS_2/CNT neural network nanostructure composite anodes for stable, high-capacity sodium-ion batteries[J]. Nano Energy, 2018, 46: 117-127.

[16] Li L, Peng S, Bucher N, et al. Large-scale synthesis of highly uniform $Fe_{1-x}S$ nanostructures as a high-rate anode for sodium ion batteries[J]. Nano Energy, 2017, 37: 81-89.

[17] Zhao Y, Wang J, Ma C, et al. Interconnected graphene nanosheets with confined FeS2/FeS binary nanoparticles as anode material for sodium-ion batteries[J]. Chemical Engineering Journal, 2019, 378: 122168.

[18] Liu T, Li Y, Zhao L, et al. In situ Fraction of carbon-Encapsulated Fe_7X_8 (X=S, Se) for Enhanced sodium storage[J]. ACS Applied Materials & Interfaces, 2019, 11:1904-190047.